Ultrahigh-*Q* mechanical oscillators through optical trapping

2012 New J. Phys. 14 045002

(http://iopscience.iop.org/1367-2630/14/4/045002)

New Journal of Physics
The open-access journal for physics

Ultrahigh-*Q* mechanical oscillators through optical trapping

D E Chang[1,2,5], **K-K Ni**[1,3], **O Painter**[1,4] **and H J Kimble**[1,3]

[1] Institute for Quantum Information and Matter, California Institute of Technology, Pasadena, CA 91125, USA
[2] ICFO—Institut de Ciencies Fotoniques, Mediterranean Technology Park, 08860 Castelldefels (Barcelona), Spain
[3] Norman Bridge Laboratory of Physics 12-33, California Institute of Technology, Pasadena, CA 91125, USA
[4] Thomas J Watson, Sr, Laboratory of Applied Physics, California Institute of Technology, Pasadena, CA 91125, USA
E-mail: darrick.chang@icfo.es

New Journal of Physics **14** (2012) 045002 (19pp)
Received 24 October 2011
Published 2 April 2012
Online at http://www.njp.org/
doi:10.1088/1367-2630/14/4/045002

Abstract. Rapid advances are being made toward optically cooling a single mode of a micro-mechanical system to its quantum ground state and observing the quantum behavior at macroscopic scales. Reaching this regime in room-temperature environments requires a stringent condition on the mechanical quality factor Q_{m} and frequency f_{m}, $Q_{\mathrm{m}} f_{\mathrm{m}} \gtrsim k_{\mathrm{B}} T_{\mathrm{bath}}/h$, which so far has been marginally satisfied only in a small number of systems. Here we propose and analyze a new class of systems that should enable one to obtain unprecedented Q-frequency products. The technique is based on the use of optical forces to 'trap' and stiffen the motion of a tethered mechanical structure, thereby freeing the resulting mechanical frequencies and decoherence rates from the underlying material properties.

[5] Author to whom any correspondence should be addressed.

Contents

The coupling of a high-Q mode of a micro-mechanical oscillator to an optical cavity has emerged as a promising route toward observing quantum behavior at macroscopic scales [1]. This opto-mechanical interaction is being used, for example, to optically cool a mechanical mode toward its quantum ground state [1–3]. Ground-state cooling requires that the product of the quality factor Q_{m} and the frequency f_{m} of the mechanical mode exceed $k_{\mathrm{B}}T_{\mathrm{bath}}/h$, where h is Planck's constant. For a room-temperature bath, this condition is marginally satisfied only in a small number of current experiments [4]. The ratio $hQ_{\mathrm{m}}f_{\mathrm{m}}/k_{\mathrm{B}}T_{\mathrm{bath}}$ also determines the quantum coherence time of the system relative to the mechanical period. Significant increases in this ratio beyond that required for ground state cooling are thus critical to prepare and detect non-classical states of motion in most optomechanical schemes (e.g., as in [5, 6]) or to store quantum information for long periods of time [7]. Mechanical systems exhibiting extremely high quality factors also offer novel opportunities for precision measurement and force detection [8, 9]. The difficulty of improving Q–frequency products, however, is highlighted by the fact that a number of systems [10, 11] already exhibit quality factors that are approaching fundamental material limits [12, 13].

In this paper, we propose a class of systems that should enable one to obtain unprecedented Q–frequency products. The approach is based on optically 'trapping' a tethered membrane with low natural mechanical frequency in the anti-node of a strong optical standing wave (see figure 1(a)) [14]. While there are many possible realizations, here we focus on a pendulum geometry where a relatively large disc is supported by a single thin tether. The dielectric disc is attracted to the anti-node of the field, leading to an optical stiffening of its flexural modes. Under realistic conditions, the re-normalized mode frequencies can be significantly enhanced over the values expected under material stresses alone. Of particular interest is the 'center-of-mass' (CM) mode, where the disc oscillates in the optical potential with negligible flexural motion. We show that this motion exhibits an extremely large ratio of potential energy stored in the optical field to strain energy, $U_{\mathrm{opt}}/U_{\mathrm{mech}}$. This is important because the optical potential is 'lossless', and the result is a correspondingly large increase in the Q–frequency product over a conventional mechanical system due to the dilution of internal friction.

Our approach to achieving long coherence times builds on previous proposals, which suggested that the highly isolated CM mode of an optically levitated nanosphere [15, 16] can

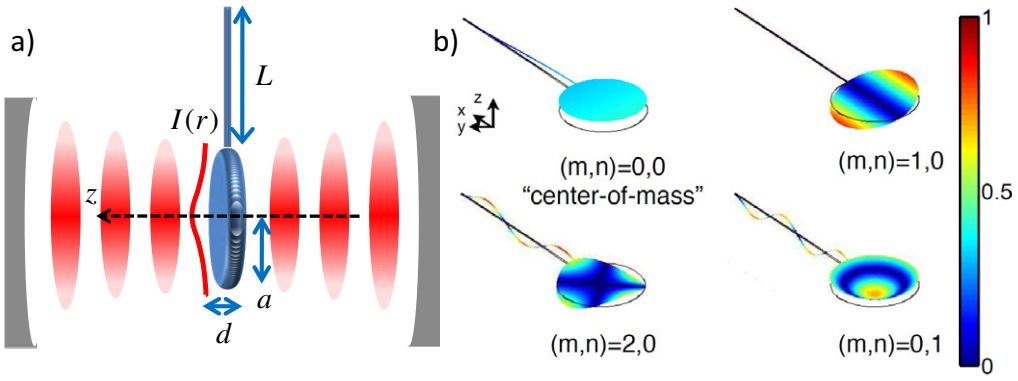

Figure 1. Illustration of a tethered membrane and its mode shapes. (a) Side view of a membrane supported by a single tether inside a Fabry–Perot cavity. The membrane has radius a and thickness d, while the tether has length L and a square cross-section of width b. It is trapped in the anti-node of a standing optical field with transverse intensity profile $I(r)$ at the membrane location. (b) Displacement fields of a few selected membrane modes (in arbitrary units) for zero trapping intensity. The black outline indicates the equilibrium position. (m, n) denote the number of nodal diameters and circles, respectively. The system dimensions are given by $a = 10\,\mu$m, $b = d = 50\,$nm and $L = 50\,\mu$m.

enable quantum opto-mechanics in room-temperature environments [17, 18]. Compared to the nanosphere, our approach has two significant advantages. Firstly, the nanosphere scatters light omni-directionally, leading to motional heating via photon recoil. Suppression of recoil heating to reach the quantum regime requires spheres with sub-wavelength volumes, $V/\lambda^3 \ll 1$ [17]. In contrast, the planar membrane primarily couples the counter-propagating components of the trapping beam, strongly reducing recoil heating even for large systems. Secondly, these membranes can be fabricated using well-established techniques that have already yielded excellent mechanical and optical properties in a number of experiments [4, 19]. Our proposal thus shows how the ideas of optical levitation can be brought to bear upon 'conventional' and practically deployable mechanical systems to yield remarkable coherence times.

This paper is organized as follows. In section 1, we develop a model for the optical forces acting on thin membranes trapped in free space, and identify the ratio of optical energy to strain energy ($U_{\rm opt}/U_{\rm mech}$) as a relevant figure of merit for enhancing Q–frequency products. We then apply these results to one particular form of dissipation, thermoelastic damping. Under realistic conditions, we show that Q–frequency product enhancements of three orders of magnitude are possible, limited by practical dimensions of the system and trapping beam. In section 2, we modify our analysis to account for trapping in a Fabry–Perot cavity. In particular, the diffraction of the optical field around the membrane causes a distortion of the cavity mode, and the optical forces must be calculated self-consistently. Scattering of the field also gives rise to photon recoil heating, an additional source of decoherence of the mechanical motion. We find that tapering or apodizing the edges of the membrane can significantly reduce photon scattering and is crucial for achieving long quantum coherence times. In section 3, the advantages of our scheme over other optical spring or trapping proposals are discussed. We conclude the paper in section 4.

1. Enhancing quality factors through optical trapping

We begin by considering the mechanical modes of a free, thin circular membrane with thickness d and radius a in the absence of any tethers. In equilibrium, the membrane is situated at $z = 0$, in the anti-node of an optical standing wave $E(z) \propto \cos kz$ (see figure 1(a)). The optical field polarizes the dielectric disc, yielding a gradient force trap around $z = 0$. In the absence of any internal forces, the optical field traps a thin membrane ($d \ll \lambda$) with a restoring frequency given by $\omega_{\rm opt}(r) = (\frac{2k^2 I(r)(\epsilon-1)}{\rho c})^{1/2}$, where r is the radial coordinate. Here $I(r)$ is the beam intensity profile (assumed to be rotationally symmetric) in the direction transverse to z, $k = 2\pi/\lambda$ is the optical wavevector, ρ is the mass density and ϵ is the dielectric constant. Now including the internal stresses, the mechanical displacement field from equilibrium, $\zeta(x, y)$, obeys

$$\frac{\partial^2 \zeta}{\partial t^2} = -\omega_{\rm opt}^2(r)\zeta - \frac{Ed^2}{12\rho(1-\sigma^2)}\nabla^4\zeta, \tag{1}$$

subject to free boundary conditions [20] (also see appendix A). E, σ denote Young's modulus and Poisson's ratio, respectively. Here and in the following, ∇^2 is understood to be the Laplacian in the transverse plane. Due to the rotational symmetry, we seek solutions of the form $\zeta(x, y) = f(r)\cos m\theta\, e^{-i\omega_m t}$. The spatial modes are indexed by the number of nodal diameters and circles, (m, n) (see figure 1(b)). For our numerical results, we take material parameters $E = 270\,\text{GPa}$, $\sigma = 0.25$, $\rho = 2.7\,\text{g cm}^{-3}$, $\epsilon = 4$ corresponding to stoichiometric silicon nitride [4], and an operating wavelength of $\lambda = 1\,\mu\text{m}$. For a free disc without optical forces, the fundamental (2, 0) flexural mode has natural frequency $\omega_{\rm m,nat}^{(2,0)}/2\pi \approx 0.25\frac{d}{a^2}\sqrt{\frac{E}{\rho(1-\sigma^2)}}$, or $\omega_{\rm m,nat}^{(2,0)}/2\pi \approx 1.3\,\text{MHz}$ for a disc of dimensions $a = 10\,\mu\text{m}$, $d = 50\,\text{nm}$. There is also a trivial solution corresponding to the CM or (0, 0) mode with constant $f(r)$ and zero frequency.

For a uniform intensity, $I(r) = I_0$, the natural radial functions $f_{\rm nat}^{(m,n)}(r)$ remain eigenmodes of equation (1), but with re-normalized mechanical frequencies given by $\omega_{\rm m}^{(m,n)}(I_0) = \sqrt{\omega_{\rm opt}^2(I_0) + (\omega_{\rm m,nat}^{(m,n)})^2}$. Thus, the CM mode is now a nontrivial solution with frequency $\omega_{\rm m}^{\rm CM} = \omega_{\rm opt}$, but still retains a uniform spatial profile. The frequencies of all the flexural modes increase as well, with the CM mode remaining the lowest in frequency (see figure 2(a)).

The absence of energy stored in internal strains for the CM motion has the important implication of eliminating dissipation due to internal friction. Instead, the energy is stored in an optical potential that contributes no losses (but can contribute a recoil heating force, as described later). So far, we have neglected the tether and have assumed a spatially uniform trapping intensity (i.e. infinite beam waist), whereas taking these factors into account prevents complete suppression of internal strain. To quantify how finite strain energy influences the mechanical quality factor, we consider the effect of thermoelastic damping on our system. We focus on thermoelastic damping, because (i) it can be analytically modeled [12, 20], (ii) it is a fundamental limit even for perfectly fabricated devices [12] and (iii) a number of micro-mechanical systems are approaching this limit [10, 11].

Thermoelastic damping arises because realistic materials have a nonzero coefficient of thermal expansion. The flexural motion creates local volume changes that then lead to temperature gradients and heat flow. Mechanical energy must be expended to drive this heat flow, leading to a finite $Q_{\rm m}$. We make two simplifying assumptions to the general thermoelastic equations [12, 20], which are well justified in our system. Firstly, we assume that the thermoelastic coupling is weak, so that the spatial modes determined by equation (1)

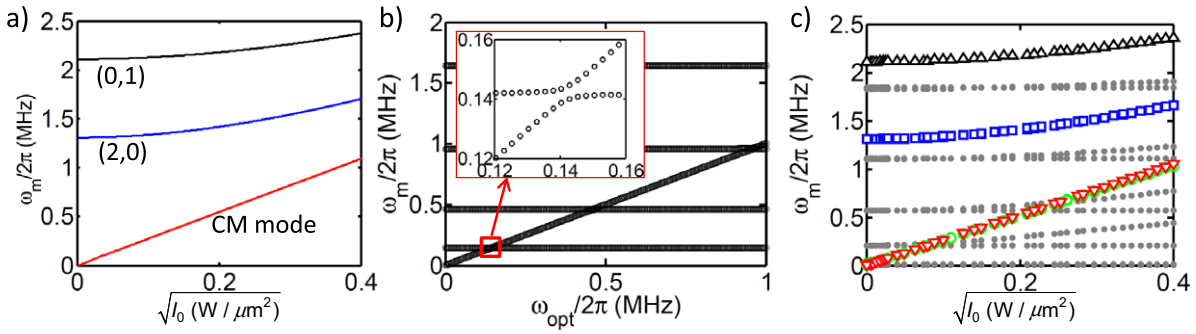

Figure 2. Frequencies of the mechanical normal modes. (a) Mode frequencies of a free circular disc trapped in an optical standing plane wave as a function of beam intensity. The disc has a thickness and a radius of $d = 50\,\text{nm}$ and $a = 10\,\mu\text{m}$, respectively, and material properties corresponding to stoichiometric silicon nitride. (b) Mode frequencies of a rigid membrane suspended by a single tether, as a function of the optical restoring frequency ω_{opt} acting on the membrane. The tether has a length of $L = 50\,\mu\text{m}$ and a square cross-section of $b = 50\,\text{nm}$ on each side, while the ratio of the membrane to tether mass is given by $M/m_{\text{t}} = 125$. Away from degeneracies, the mode spectrum consists of a CM mode with frequency $\sim\omega_{\text{opt}}$ and discrete tether modes with frequencies ω_n ($n = 1, 2, 3, \ldots$). Avoided crossings occur near degeneracies $\omega_{\text{opt}} \sim \omega_n$ (see the inset). (c) Mode frequencies for a realistic tethered system, as a function of peak trapping beam intensity. The disc and tether have dimensions identical to those in (a) and (b), while the beam waist is $w = 35\,\mu\text{m}$. The gray points indicate tether modes. The red (▽), green (○), blue (□) and black (△) points denote the CM, (1, 0), (2, 0) and (0, 1) membrane modes, respectively.

are not altered to lowest order. Secondly, the strains vary most rapidly along the thin direction of the disc, and thus we ignore the relatively small transverse temperature gradients. The temperature field is given by $T(x, y, z, t) = T_{\text{bath}} + \Delta T(x, y, z, t)$, where ΔT satisfies the driven heat equation

$$\left(c_V \frac{\partial}{\partial t} - \kappa_{\text{th}} \frac{\partial^2}{\partial z^2}\right) \Delta T = \frac{E\alpha T_{\text{bath}} z}{3(1-2\sigma)} \frac{\partial}{\partial t} \nabla^2 \zeta \tag{2}$$

with boundary conditions $\partial \Delta T/\partial z = 0$ at $z = \pm d/2$. Here c_{V} is the heat capacity per unit volume, κ_{th} is the thermal conductivity and α is the volumetric thermal expansion coefficient (we take $c_{\text{V}} = 2\,\text{J}\,\text{cm}^{-3}\,\text{K}$, $\kappa_{\text{th}} = 20\,\text{W}\,\text{m}\,\text{K}$ and $\alpha = 4.8 \times 10^{-6}\ \text{K}^{-1}$ for SiN). The work done in driving the heat flow over one cycle is

$$\Delta W \approx -\frac{\kappa_{\text{th}}}{T_{\text{bath}}} \int_0^{2\pi/\omega_{\text{m}}} \text{d}t \int \text{d}^3\mathbf{r} \Delta T(\mathbf{r})(\partial^2 \Delta T/\partial z^2), \tag{3}$$

and the thermoelastically limited quality factor is $Q_{\text{m,th}} = 2\pi(U_{\text{opt}} + U_{\text{mech}})/\Delta W$, where U_{opt} and U_{mech} are the energies stored in the optical field and strains, respectively. To good approximation, one finds that the thermoelastically limited Q–frequency product is given by $Q_{\text{m,th}} f_{\text{m}} = \frac{45\kappa_{\text{th}}}{\pi E d^2 T_{\text{bath}} \alpha^2} \frac{1-\sigma}{1+\sigma}(1 + U_{\text{opt}}/U_{\text{mech}})$ (see appendix B). Thus, the storage of energy in the optical field leads directly to an enhancement of the Q–frequency product. As a

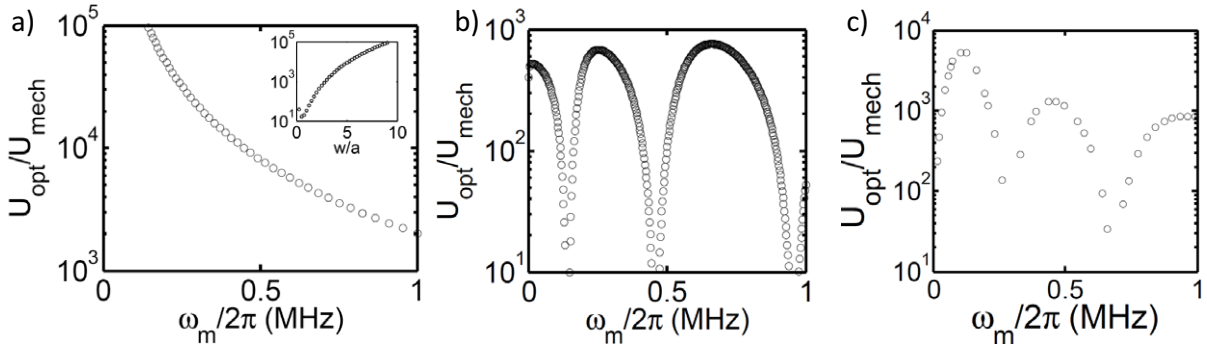

Figure 3. The ratio $U_{\rm opt}/U_{\rm mech}$ of optical energy to strain energy for the CM mode of different systems: (a) an optically trapped free disc as a function of its frequency $\omega_{\rm m}/2\pi$. Here the beam waist is fixed at $w = 35\,\mu$m and the trap intensity is varied to yield the corresponding $\omega_{\rm m}$. Inset: the trap intensity is fixed such that $\omega_{\rm m}/2\pi = 1$ MHz in the plane wave limit while w/a is varied. (b) A rigid membrane suspended by a single tether, as a function of the CM frequency. (c) A realistic tethered structure, obtained by finite-element simulations. The system dimensions for these plots are identical to those in figure 2, namely, $a = 10\,\mu$m, $L = 50\,\mu$m and $d = b = 50$ nm.

useful comparison, in the absence of optical trapping, an unstressed stoichiometric SiN film of thickness $d = 50$ nm would have a Q–frequency product limited to $Q_{\rm m,th} f_{\rm m} \approx 4 \times 10^{13}$ Hz at room temperature, which only marginally exceeds the fundamental limit $k_{\rm B} T_{\rm bath}/h \approx 6 \times 10^{12}$ Hz needed for ground-state cooling. The Q–frequency product is also proportional to the number of coherent oscillations that the system can undergo before a single phonon is exchanged with the thermal bath, $N_{\rm th}^{\rm (osc)} = Q_{\rm m,th} f_{\rm m} h/(2\pi k_{\rm B} T_{\rm bath})$ ($N_{\rm th}^{\rm (osc)} \sim 1$ for the conventional membrane described above). A large value is critical for preparing and observing quantum superposition or entangled states [5, 6].

We now examine thermoelastic damping of our free disc. Clearly, if $\omega_{\rm opt}(r)$ is spatially uniform, the CM mode has no internal strains and experiences zero thermoelastic dissipation. A finite beam waist creates inhomogeneous optical forces that internal stresses must compensate for, which mixes CM and internal motion together (we still refer to this mixed mode as the 'CM'). The mixing becomes significant when the variation in $\omega_{\rm opt}(r)$ across the disc overtakes the natural rigidity of the system (as characterized by the natural fundamental frequency), and can be avoided by using sufficiently large beam waists or low intensities. In this regime, significant enhancements to the Q–frequency product should result.

These effects are illustrated in figure 3(a). For concreteness, we assume that the trapping beam has a Gaussian profile with waist w, $I(r) = I_0\, {\rm e}^{-2r^2/w^2}$ (for now, we ignore possible corrections due to distortion as the beam diffracts around the disc). In figure 3(a), we plot the ratio $U_{\rm opt}/U_{\rm mech}$ for the CM mode as a function of its frequency, which is varied through the peak intensity I_0. We use the same disc dimensions as before and a waist of $w = 35\,\mu$m. The energy ratio monotonically decreases, reflecting the increased inhomogeneity in the optical potential. In the inset, a complementary process is illustrated, where the beam waist w is varied, while the peak intensity I_0 is fixed such that $\omega_{\rm opt}(I_0)/2\pi = 1$ MHz. The energy ratio increases indefinitely with w/a and approaches infinity in the plane-wave limit.

We now consider the realistic pendulum geometry shown in figure 1(a), where the tether provides an extremely weak restoring force for the 'CM' motion of the disc. We first present a simplified analysis that isolates the role of the tether in the mode spectrum and Q–frequency product. Specifically, we treat the membrane as a perfectly rigid point particle of mass M, which experiences an optical restoring force with frequency $\omega_{\rm opt}$, while internal stresses alone act on the tether. Then, for a tether of length L whose long axis is situated along x, the displacement field $\phi(x,t)$ (where $0 \leqslant x \leqslant L$) satisfies the beam equation [20]

$$\frac{\partial^2\phi}{\partial t^2} = -\frac{Eb^2}{12\rho}\frac{\partial^4\phi}{\partial x^4}. \tag{4}$$

Here b denotes the width of the tether (assumed to be square in cross-section). The beam is clamped at $x=0$, $\phi(0,t)=\partial_x\phi(0,t)=0$, while at $x=L$ the boundary conditions are given by $\partial_x^2\phi(L,t)=0$ and $M\partial_t^2\phi(L,t) = -M\omega_{\rm opt}^2\phi(L,t) + Eb^4\partial_x^3\phi(L,t)/12$. The last equation describes the acceleration of the membrane due to optical restoring forces and the shear force imparted by the tether.

It is straightforward to solve for the system eigenmodes and the results are summarized here. For large mass ratios between the membrane and tether, $M/m_{\rm t}\to\infty$, the modes usually consist of a CM mode for the membrane with frequency $\omega_{\rm m}^{\rm CM} \approx \sqrt{\omega_{\rm p}^2+\omega_{\rm opt}^2}$ and a set of discrete tether modes with frequencies $\omega_n \approx (\frac{(n+1/4)\pi}{\beta L})^2$, where $\beta = (12\rho/Eb^2)^{1/4}$. The CM mode spectrum is understood as a low-frequency 'pendulum' mode (with natural frequency $\omega_{\rm p}\approx\sqrt{Eb^4/4ML^3}$, where $\omega_{\rm p}\ll\omega_{\rm opt},\omega_n$ for our systems of interest) whose frequency can be strongly re-normalized by the optical force, while the tether mode spectrum results from the heavy membrane essentially acting as a second clamp. This description holds except near degeneracies $\omega_{\rm opt}\approx\omega_n$, where coupling between the tether and membrane motions yields an avoided crossing whose width decreases with increasing mass ratio $M/m_{\rm t}$. This result is illustrated in figure 2(b), for a mass ratio of $M/m_{\rm t}=125$ (corresponding to the disc size considered earlier attached to a tether of length $L=50\,\mu$m and width $b=50$ nm). In figure 3(b), we plot the energy ratios $U_{\rm opt}/U_{\rm mech}$ for the CM motion as a function of $\omega_{\rm opt}$. Here, the strain energy is completely attributable to the tether, as we take the membrane to be a rigid object. The energy ratio is dramatically reduced near the avoided crossings, while away from these crossings, the energy ratio plateaus to a value near $U_{\rm opt}/U_{\rm mech}\sim 8M/m_{\rm t}$.

For a realistic tethered system (as in figure 1(a)) where the membrane is not perfectly rigid, mode mixing between the tether and membrane and mixing between the CM and internal membrane motion will occur simultaneously. We have numerically solved the full stress–strain equations for such a system using COMSOL, a commercial finite-element simulation package. A characteristic mode spectrum is plotted in figure 2(c) as a function of the peak trapping intensity I_0, for parameters $a=10\,\mu$m, $L=50\,\mu$m, $d=b=50$ nm and $w=35\,\mu$m. Away from avoided crossings, the modes can clearly be characterized as tether modes (gray points) or membrane modes (color). For our particular choice of beam waist size, the tethers themselves experience optical restoring forces, leading to a slight optical stiffening of tether modes that have displacements along the optical propagation axis. Comparing the membrane modes, the CM mode lies lower in frequency than the flexural modes, as in the case of a free disc. A nearly degenerate torsional $(1,0)$ mode also exists, which in principle should have no opto-mechanical coupling to the cavity field and can be ignored.

In figure 3(c), we plot the energy ratio $U_{\rm opt}/U_{\rm mech}$ for the CM mode of our tethered structure as a function of its frequency. The features displayed here are clearly a combination of those

appearing in the limiting cases of a free disc and a rigid disc attached to a tether. In particular, large plateaus in $U_{\rm opt}/U_{\rm mech}$ appear away from avoided crossings with tether modes. The plateau heights can be higher than the limit $U_{\rm opt}/U_{\rm mech} \sim 8M/m_{\rm t}$ predicted by the simple model, since the tether experiences an optical spring force as well. The decrease in the plateau heights with increasing CM frequency is associated with increased mixing between pure CM and internal membrane motion. For the realistic geometry considered here, an enhancement in the Q–frequency product of the order of $\sim 10^3$ compared to a conventional system can be realized at a frequency of $\omega_{\rm m}/2\pi \sim 1\,$MHz. For a thermoelastically limited system, this corresponds to a coherence time of $N_{\rm th}^{(\rm osc)} \sim 10^3$.

Although we have focused on thermoelastic processes, which can be exactly modeled, we emphasize that our conclusions are qualitatively correct for any internal dissipative process. For example, a number of other mechanical systems phenomenologically suffer from frequency-independent dissipation, which may be due to effects such as tunneling in amorphous solids [13] or surface mechanisms [21]. Such systems can be characterized by a complex, frequency-independent Young's modulus $E = E_r + {\rm i}E_i$, where the imaginary component accounts for dissipation of strain energy. In this case, the quality factor in the presence of optical trapping behaves like $Q_{{\rm m},E} = (E_r/E_i)(1 + U_{\rm opt}/U_{\rm mech})$, again indicating the importance of storing energy in the lossless optical potential.

2. A membrane in a cavity: modification of modes and recoil heating

So far, we have assumed that the trapping beam has a Gaussian profile. For cavity optomechanics [1], it will be necessary to trap the membrane within a Fabry–Perot cavity, as illustrated in figure 1(a). For example, here, a relatively strong beam could be used for trapping, while a second, weaker beam with a nonzero intensity gradient at the trap position would facilitate cooling of the CM motion or quantum state transfer processes [17, 18]. The membrane scatters and diffracts the cavity light, which introduces two important effects. Firstly, the mode will no longer be Gaussian, and the new optical mode accommodated by the cavity mirrors and the corresponding optical forces must be determined. Secondly, photon scattering out of the cavity reduces cavity finesse, and the associated random momentum kicks ('photon recoil') imparted on the membrane lead to additional decoherence.

To quantify these effects, we begin by calculating the cavity modes in the presence of the membrane using a modified Fox–Li propagation technique [22]. Here, the electric field is treated within the scalar paraxial approximation, and thus it is completely described by its transverse profile $E(x, y)$. This approximation is justified by noting that the disc should primarily diffract light at small angles $\theta \lesssim (ka)^{-1}$ around the z-axis, where $k = 2\pi/\lambda$ is the optical wavevector. Within this approximation, free propagation over a distance z is accounted for by a phase shift in the Fourier transform of the field profile, $\tilde{E}(k_x, k_y) \to {\rm e}^{{\rm i}kz - {\rm i}(k_x^2 + k_y^2)z/(2k)}\tilde{E}(k_x, k_y)$. In our case, we are interested in systems with rotational symmetry, and thus the transforms are implemented through the quasi-discrete Hankel transform described in [23]. Reflection off a circular mirror with radius of curvature $R_{\rm c}$ and reflectance $R_{\rm m}$ is characterized by the real-space transformation $E(x, y) \to \sqrt{R_{\rm m}}E(x, y)\exp\left(2{\rm i}\,k(R_{\rm c} - \sqrt{R_{\rm c}^2 - (x^2 + y^2)})\right)$. Similarly, at the membrane location, the wave front can undergo reflection and transmission. In the case of an infinite dielectric membrane of uniform thickness d, the Fresnel equations yielding the thickness-dependent

reflection and transmission coefficients $r(d)$, $t(d)$ can be exactly solved. Following the Fox–Li technique, for a finite-size membrane or a membrane of non-uniform thickness, we apply these expressions to approximate the scattering amplitude and phase shift locally. For example, a field $E(x, y)$ incident on the membrane undergoes the transformation $E(x, y) \rightarrow t(d(x, y))E(x, y)$ upon transmission. Note that an initial wave front incident on the membrane thus splits into two wave fronts (a reflected and a transmitted field), and we keep track of the multiple scattered fields to all orders to calculate the field buildup or cavity eigenmodes. In contrast, the original technique of [22] only accounts for transmission. Thus, our approach properly captures the effects of the reflected amplitude and back-scattered angle. Furthermore, our modified technique reveals specifically at what frequencies resonances should occur.

We now discuss the effect of the membrane on the cavity finesse. To speed up calculations (taking advantage of the rotational symmetry) and given the relatively small size of the tether, only the central disc is treated here. As realistic parameters, we consider a membrane placed symmetrically in the center of an optical cavity of length $L = 1.99\,\mathrm{cm}$ with spherical mirrors having radii of curvature $R_\mathrm{c} = 1\,\mathrm{cm}$ and perfect reflectivity (such that we can identify the contribution κ_mem to the cavity linewidth due to scattering from the membrane). The transverse extent of the spherical mirror surfaces is $r_\mathrm{m} = 0.95\,\mathrm{mm}$, i.e. all portions of the beam front with $x^2 + y^2 > r_\mathrm{m}^2$ are scattered out and set to zero upon reflection at the mirror. Accounting for a realistic mirror extent is important in determining the scattering rate, as a fully enclosing mirror would be a closed system and would exhibit no losses. An empty cavity in this configuration yields a Gaussian mode of waist $w_0 \approx 15\,\mu\mathrm{m}$ in the center. In figure 4(a), we plot the membrane-limited cavity finesse $\mathcal{F}_\mathrm{mem} \equiv \pi c/\kappa_\mathrm{mem} L$ for a membrane of uniform thickness $d = 30\,\mathrm{nm}$ and varying radius a (black circles). Clearly, cavity losses are negligible when the nominal waist is small compared to the disc radius, $w_0/a \lesssim 1$. In the regime $w_0/a \gtrsim 1$, however, the finesse rapidly drops, which is attributable to scattering by the hard edges of the disc. This effect is strongly reduced by 'softening' or apodizing the disc edge [24]. In figure 4(a) (red circles), we also plot the finesse for a membrane whose thickness $d(r) = d_0(1 - (r/a)^2)^2$ tapers down to zero at the edge, where $d_0 = 30\,\mathrm{nm}$ is the maximum thickness. Remarkably, the apodization can improve the cavity finesse by several orders of magnitude. The modification of the cavity modes by the membrane is illustrated in figure 4(b), where we plot the transverse profile at the membrane position for some representative apodized disc sizes.

We find the CM eigenmodes of the apodized disc using equation (A.3), which is a generalization of equation (1) to a disc of non-uniform thickness. The optical potential $\omega_\mathrm{opt}(r)$ is now evaluated using the modified cavity mode profiles. The thermoelastic limit is subsequently calculated using equations (2) and (3). In figure 4(c), the number of oscillations $N_\mathrm{th}^{(\mathrm{osc})}$ due to thermoelastic damping is plotted (in black). Here the circulating intra-cavity power is chosen such that the CM frequency is fixed at $\omega_\mathrm{m}/2\pi = 0.5\,\mathrm{MHz}$.

We next consider the effect of photon recoil heating. We assume that each scattered photon contributes the maximum possible momentum kick of $\hbar k$ along the z-axis, giving rise to a momentum diffusion process $\mathrm{d}\langle p_z^2\rangle/\mathrm{d}t = (\hbar k)^2 R_\mathrm{sc}$ [17], where R_sc is the photon scattering rate. Converting this expression into a jump rate, it can be shown that the number of coherent oscillations before a jump in the phonon number can be written as

$$N_\mathrm{sc}^{(\mathrm{osc})} = \frac{1}{2\pi}\frac{V}{V_\mathrm{c}}\frac{\omega_0}{\kappa}\frac{\omega_\mathrm{m}^2}{k^2 I_\mathrm{max}/\rho c}. \tag{5}$$

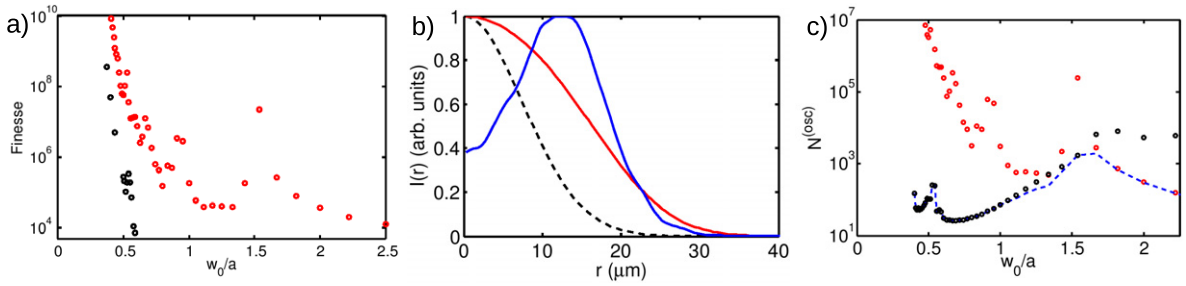

Figure 4. Effects of optical scattering from a membrane inside a cavity. (a) Membrane-limited finesse $\mathcal{F}_{\rm mem}$ of a Fabry–Perot cavity with a membrane in the middle. The black circles correspond to a flat membrane of uniform thickness $d = 30\,\text{nm}$, while the red circles correspond to an apodized membrane with maximum thickness $d_0 = 30\,\text{nm}$. The finesse is plotted as a function of the ratio of the empty-cavity beam waist w_0 to the membrane radius a. The cavity parameters are chosen such that $w_0 = 15\,\mu\text{m}$. (b) Intensity profiles (in arbitrary units) of cavity mode in the presence of an apodized membrane. The intensity profile is evaluated halfway between the two cavity mirrors. The cavity and membrane parameters are provided in the main text. The blue and red curves correspond to disc radii $a = w_0$ and $a = 2.5w_0$, respectively, while the dashed black curve is the Gaussian intensity profile for an empty cavity. (c) The number of coherent oscillations of the CM motion of an apodized disc due to thermoelastic damping ($N_{\rm th}^{(\rm osc)}$, black cirlces) and recoil heating ($N_{\rm sc}^{(\rm osc)}$, red circles), as a function of disc radius and for fixed $w_0 = 15\,\mu\text{m}$. Also plotted is the total number of coherent oscillations ($N_{\rm tot}^{(\rm osc)}$, blue dashed curve), which is given by the sum in parallel of the individual contributions.

Here $I_{\rm max}$ is the maximum cavity intensity (which in general does not need to be at the center of the membrane due to mode distortion), $\omega_0 = ck$, V is the volume of the disc and $V_{\rm c}$ is the cavity mode volume. Assuming that the cavity mode is not significantly distorted and that the beam waist $w_0 \gtrsim a$ such that the entire membrane experiences the optical force, one can approximate $\frac{\omega_{\rm m}^2}{k^2 I_{\rm max}/\rho c} \sim 1$ and $V_{\rm c} \sim \pi w_0^2 L/4$. In this case, the number of coherent oscillations scales roughly as $N_{\rm sc}^{(\rm osc)} \sim \frac{kV}{w_0^2}\mathcal{F}_{\rm mem}$. Note that this result is purely geometric in nature and also scales directly with the cavity finesse (which itself depends on V). In figure 4(c), we plot $N_{\rm sc}^{(\rm osc)}$ for the apodized disc (in red). Combining the effects of thermoelastic damping and recoil heating, the total number of coherent oscillations is given by $N_{\rm tot}^{(\rm osc)} = (N_{\rm sc}^{(\rm osc)-1} + N_{\rm th}^{(\rm osc)-1})^{-1}$ (blue curve). It can be seen that an apodized disc of radius $r \sim 9\,\mu\text{m}$ can support a coherence time of $N_{\rm tot}^{(\rm osc)} \sim 2000$ in a room-temperature environment. Remarkably, the coherence time of this system is comparable to that of a much smaller levitated nanosphere of radius $r \sim 25\,\text{nm}$ [17], or a conventional 1 MHz oscillator with $Q_{\rm m}$ exceeding 10^8 at a bath temperature of 1 K. In appendix D, we provide an example set of parameters for this system, demonstrating that it can be cooled to the quantum ground state.

Our analysis so far presents the limitations imposed on the system due to the trapping mode. If a separate mode at a nearby frequency is used for optomechanical coupling and cooling, one should expect similar effects (e.g. finesse limitation and mode distortion) for this secondary

mode as well. We note, however, that it should also be possible to separately optimize the parameters such as finesse, beam waist and effective cavity length for the two modes by using significantly different wavelengths or compound cavity geometries.

3. Comparison of optical trapping schemes

We emphasize that our approach to reach the quantum regime, which relies upon achieving ultrahigh-Q factors, is fundamentally different from other 'optical spring' proposals based on optical backaction forces [25, 26]. In the latter case, the linear coupling of the mechanical displacement to the intra-cavity intensity can yield a dynamic optical spring effect. This effect, however, is accompanied by significant Raman scattering of the optical pump field, which causes phonons to be rapidly removed and added to the system. While this does not preclude ground state cooling [26], our analysis below demonstrates that it imposes severe limitations on the quantum coherence time and makes it difficult to prepare, e.g., quantum superposition states. In contrast, in our scheme, the phonons are truly long-lived excitations.

Specifically, we consider the dynamic optical spring resulting from a mechanical degree of freedom whose displacement is linearly coupled to the optical cavity frequency. The corresponding Hamiltonian for such a system in a rotating frame is [27]

$$H_{\rm int} = \frac{\hat{p}^2}{2m} + \frac{1}{2}m\omega_{\rm m}^2\hat{z}^2 - \hbar\delta\hat{a}^\dagger\hat{a} - \hbar\omega'\hat{z}\hat{a}^\dagger\hat{a} - \hbar\Omega_L(\hat{a}+\hat{a}^\dagger). \tag{6}$$

Here $\hat{a}$ is the annihilation operator for the optical mode, $\hat{z}$, $\hat{p}$ are the position and momentum operators corresponding to the mechanical resonator, $\omega_{\rm m}$ is the natural mechanical frequency, $\delta = \omega_L - \omega_0$ is the frequency detuning between an external pump field driving the optical cavity and the optical resonance frequency ω_0 (when the mechanical resonator is in equilibrium), Ω_L is the driving amplitude and ω' is the optical cavity frequency shift per unit mechanical displacement. In addition to the Hamiltonian terms, the optical cavity is assumed to have losses characterized by a linewidth κ.

For weak opto-mechanical coupling, it is customary to linearize the optical cavity dynamics around the classical steady-state value $\langle\hat{a}\rangle = \alpha = \mathrm{i}\,\Omega_L/(\kappa/2 - \mathrm{i}\,\delta)$ (here we have incorporated a steady-state shift of the optical resonance frequency into our definition of the detuning δ), and eliminate the cavity to yield an effective susceptibility $\chi(\omega)$ of the mechanical displacement in response to an external force $f(\omega)$ [27]. Specifically, one finds that

$$\chi(\omega)^{-1} = \omega_{\rm m}^2 - \omega^2 + \frac{16\omega_{\rm m}\delta\Omega_{\rm m}^2}{4\delta^2 + (\kappa - 2\mathrm{i}\omega)^2}. \tag{7}$$

Here we have defined an effective opto-mechanical driving amplitude $\Omega_{\rm m} = g\alpha$, and $g = \omega' z_{\rm zp} = \omega'\sqrt{\frac{\hbar}{2m\omega_{\rm m}}}$ is the optical cavity frequency shift per unit mechanical zero-point uncertainty. In the perturbative limit, this expression can be written in terms of the susceptibility of a simple oscillator with an effective linewidth and frequency that is modified due to opto-mechanical interactions, $\chi(\omega)^{-1} \approx \omega_{\rm m,eff}^2 - \omega^2 - \mathrm{i}\,\omega\Gamma_{\rm eff}$. The effective linewidth and mechanical frequency shift can be interpreted as resulting from optically induced cooling (or heating) and a dynamic optical spring constant, respectively. In the relevant regime of large detuning $\delta \gg \omega, \kappa$, and when the optical spring is dominant compared to the natural mechanical frequency, the effective

mechanical frequency is given by [27, 28]

$$\omega_{\mathrm{m,eff}} \approx 2\Omega_{\mathrm{m}}\sqrt{\frac{\omega_{\mathrm{m}}}{\delta}}. \tag{8}$$

The damping rate is given by

$$\Gamma_{\mathrm{eff}} \approx \Omega_{\mathrm{m}}^2\kappa\frac{\omega_{\mathrm{m}}}{\omega_{\mathrm{m,eff}}}\left[\frac{1}{(\kappa/2)^2+(\delta+\omega_{\mathrm{m,eff}})^2}-\frac{1}{(\kappa/2)^2+(\delta-\omega_{\mathrm{m,eff}})^2}\right], \tag{9}$$

which is interpreted as the difference between anti-Stokes and Stokes scattering rates. Note that for positive detuning $\delta > 0$, the opto-mechanical interaction yields an increase in the mechanical frequency but an anti-damping force ($\Gamma_{\mathrm{eff}} < 0$). One can achieve simultaneous stiffening and cooling by employing multiple beams with different amplitudes and detunings [26], but for our purposes it is sufficient to consider only the beam that leads to stiffening.

We wish to consider the ratio of the effective mechanical frequency to the rate of decoherence Γ_{d} induced by optical Raman scattering, which is given by the sum (and not difference) of the anti-Stokes and Stokes scattering rates. This is an important point—although the removal and addition of a phonon by two Raman scattering events has no net effect in terms of energy, it does destroy quantum coherence. In the relevant limit of large detuning and dominant optical spring effect, one finds that

$$\frac{\omega_{\mathrm{m,eff}}}{\Gamma_{\mathrm{d}}} \approx \frac{2\delta}{\kappa}. \tag{10}$$

This result states that the cavity must be driven very far off resonance in order to yield a frequency shift that is much larger than the decoherence rate. Operating at large detuning in turn requires extremely large cavity input powers to get an appreciable optical spring effect. As an example, we consider the dynamic spring constant for a realistic geometry, such as a Fabry–Perot cavity of length $L = 1\,\mathrm{cm}$ and cavity finesse $\mathcal{F} = 10^5$ (with the cavity linewidth given by $\kappa = \pi c/(\mathcal{F}L) = 2\pi\times 150\,\mathrm{kHz}$ for our specific parameters). The optical driving amplitude is related to the input power P_{i} through $\Omega_L = \sqrt{\kappa P_{\mathrm{i}}/(2\hbar\omega_L)}$ for perfect in-coupling efficiency, while the opto-mechanical interaction strength is of order $\omega' \sim \omega_0/L$. The operating wavelength is taken to be $\lambda = 1\,\mu\mathrm{m}$. We also assume that the SiN membrane has a radius $a = 10\,\mu\mathrm{m}$ and that it undergoes pure CM motion (such that its effective motional mass is the same as the physical mass). Then, an input power of $P_{\mathrm{i}} \sim 2\,\mathrm{kW}$ is required if one wants to achieve the number of coherent oscillations of $N^{(\mathrm{osc})} = \frac{\omega_{\mathrm{m,eff}}}{2\pi\Gamma_{\mathrm{d}}} \sim 10^3$ and an effective mechanical frequency of $\omega_{\mathrm{m,eff}} \sim 2\pi\times 1\,\mathrm{MHz}$. This corresponds to an input intensity of $\sim 10\,\mathrm{W}\,\mu\mathrm{m}^{-2}$ for a beam focused to a size comparable to the membrane radius.

In contrast, in our static trapping scheme, a comparable mechanical frequency and coherence time can be achieved for an *intra-cavity* intensity of $\sim 0.1\,\mathrm{W}\,\mu\mathrm{m}^{-2}$, and the cavity can be driven resonantly to facilitate the intra-cavity field buildup. Because the static trap results in the membrane being trapped at an anti-node, there is no linear opto-mechanical coupling for the trapping field and the lowest-order opto-mechanical coupling is quadratic in nature. The anti-Stokes and Stokes scattering rates in this case (at frequencies $\omega_L \pm 2\omega_{\mathrm{m}}$) have been calculated in [29] and are extremely rare for our realistic systems (occurring at a sub-Hz level), leading to negligible decoherence.

Furthermore, regardless of the trapping scheme used, our analysis properly captures the role that strong, spatially non-uniform optical forces have in mixing internal motion, which is neglected in lowest-order opto-mechanical models but is relevant to most flexural systems. In

the case of the dynamic optical spring, for example, our model shows that the opto-mechanical coupling strength g decreases significantly at the large intensities needed to observe strong optical spring effects (see appendix C).

We also point out the proposal in [30] that is qualitatively similar to ours, which involves the optical levitation of a macroscopic mirror using dipole forces. We believe that their conclusion of the feasibility of levitating such a macroscopic system is based on a number of erroneous assumptions. Specifically, their expression for the trapping force is derived from the optical polarizability of a sub-wavelength particle. In this regime, both the trapping force and mass increase linearly with the volume of the particle, and thus the CM oscillation frequency remains size independent for a fixed intensity. However, for objects greater than a wavelength, the ratio of trapping force to mass decreases (inversely with thickness, for the case of a planar structure [31]), and thus the authors of [30] greatly underestimate the power requirements for trapping a macroscopic mirror. In contrast, our membranes remain thin along the trapping axis, which allows for sub-wavelength formulae to hold. Furthermore, their calculation of the recoil heating rate only accounts for scattering from thermal density fluctuations (this mechanism is important for guided modes in a low-loss fiber) [32]. However, this ignores the large scattering cross-section of the externally illuminated dielectric object. Indeed, it has been shown previously that wavelength-scale particles already suffer severe decoherence times ($N_{\mathrm{sc}}^{(\mathrm{osc})} \sim 1$) due to this effect [17]. This mechanism is suppressed in our scheme because of our planar geometry and the use of a cavity mode to trap, which enables the cavity mirrors to re-capture much of the scattered light.

4. Conclusion and outlook

We have described a technique that allows the ideas of optical levitation to be applied to conventional, scalable mechanical systems, yielding Q–frequency products significantly higher than what material properties would nominally dictate. Although we have focused on thermoelastic losses in the above calculations, we expect similar improvements for any other internal damping mechanism. The key idea is that it is possible to circumvent natural material limits of damping by storing energy in a lossless optical field rather than the internal strain. By making the ratio of these energies large, $U_{\mathrm{opt}}/U_{\mathrm{mech}} \gg 1$, any internal losses can be suppressed by a corresponding degree. This fundamental observation allows one to design a novel class of mechanical systems that can be fabricated and deployed using conventional techniques, yet yield Q–frequency products that are several orders of magnitude higher than previous systems. We believe that this work will stimulate further investigation into the relationship between optical forces and material dissipation in a number of systems where the mechanical motion can be strongly renormalized by light [26, 33]. Furthermore, we anticipate that such studies will open up interesting possibilities for quantum manipulation of mechanical systems in room-temperature environments.

Acknowledgments

The authors thank Dal Wilson and Richard Norte for many helpful discussions. DEC acknowledges support from the NSF (grant no. PHY-0803371), the Gordon and Betty Moore Foundation through Caltech's Center for the Physics of Information (CPI), and Fundació Privada Cellex Barcelona. KN acknowledges support from the CPI. HJK and OJP acknowledge

support from the DARPA ORCHID program. HJK also acknowledges support from the NSF and DoD National Security Science and Engineering Faculty Fellowships (NSSEFF) program.

Appendix A. Derivation of the membrane equation

Here we derive the equation of motion for a thin non-uniform disc of thickness $d(r)$, which has a reflection symmetry around $z = 0$ (such that the surface of the plate is located at $z = \pm d(r)/2$). We are interested in the situation where the thickness is much less than the characteristic transverse size (e.g. the radius a of a circular disc), such that its degree of freedom along the thin direction can be effectively eliminated and the flexural motion can be described by a two-dimensional displacement field $\zeta(x, y)$. The equation of motion for $\zeta(x, y)$ can be obtained by a generalization of the derivation for a uniform disc given in [20]. Specifically, the energy associated with the displacement field $\zeta(x, y)$ is given by

$$U_{\text{mech}} = \frac{E}{24(1-\sigma^2)} \int \mathrm{d}x\, \mathrm{d}y\, \mathrm{d}(x, y)^3 \left[\left(\zeta_{xx} + \zeta_{yy}\right)^2 + 2(1-\sigma)\left((\zeta_{xy})^2 - \zeta_{xx}\zeta_{yy}\right)\right]. \tag{A.1}$$

Here E, σ are the Young's modulus and Poisson's ratio, respectively, while $\zeta_{xx} = \frac{\partial^2 \zeta}{\partial x^2}$, etc. To derive the equilibrium field $\zeta(x, y)$ under some external normal pressure $P(x, y)$, we employ the variational principle to minimize the system energy. Under small variations $\delta\zeta$ and following some algebra, the variation in U_{mech} can be written as the sum of an integral over the transverse area of the disc and two integrals over the circumference or edge of the disc,

$$\delta U_{\text{mech}} = \int \mathrm{d}x\, \mathrm{d}y\, Z_1 \delta\zeta + \oint \mathrm{d}l\, Z_2 \frac{\partial \delta\zeta}{\partial n} + \oint \mathrm{d}l\, Z_3 \delta\zeta. \tag{A.2}$$

Here Z_i are complicated expressions involving ζ and $d(r)$ whose forms are given below, while n denotes the normal to the edge of the disc. The integral over the disc area yields the equilibrium equation of the disc, $Z_1 = P(x, y)$, or the dynamical equation can be obtained by replacing $P(x, y) \to -\rho d(r) \frac{\partial^2 \zeta}{\partial t^2}$. Doing so, and including the effect of external optical forces, one finds that

$$\frac{\partial^2 \zeta}{\partial t^2} = -\omega_{\text{opt}}^2(r)\zeta - \frac{E}{12\rho(1-\sigma^2)d(r)} \left[\nabla^2 \left(g(r)\nabla^2\zeta\right) - (1-\sigma)\left(\zeta_{yy}g_{xx} + \zeta_{xx}g_{yy} - 2\zeta_{xy}g_{xy}\right)\right]. \tag{A.3}$$

Here we have defined $g(r) = d(r)^3$, and ∇^2 is understood to be the Laplacian in the transverse plane. As described in the main text, $\omega_{\text{opt}}(r) = (\frac{2k^2 I(r)(\epsilon-1)}{\rho c})^{1/2}$. For a disc with free boundary conditions at the edge, the quantities $\delta\zeta$ and $\partial\delta\zeta/\partial n$ are arbitrary on the boundary, so the coefficients $Z_{2,3}$ should vanish, yielding the two boundary conditions. Defining n and l to be the normal and tangential directions to the edge of the disc, and θ as the local angle between x and n, these boundary conditions become

$$\begin{aligned} 0 = {} & \frac{\partial}{\partial n}\left(g\nabla^2\zeta\right) + (1-\sigma)\left[\frac{\partial}{\partial l}\left(-g\zeta_{xy}\cos 2\theta + (g/2)\sin 2\theta(\zeta_{xx} - \zeta_{yy})\right)\right. \\ & \left. + \cos\theta(\zeta_{yy}g_x - \zeta_{xy}g_y) + \sin\theta(\zeta_{xx}g_y - \zeta_{xy}g_x)\right], \\ 0 = {} & \nabla^2\zeta + (1-\sigma)\left(2\zeta_{xy}\sin\theta\cos\theta - \zeta_{yy}\cos^2\theta - \zeta_{xx}\sin^2\theta\right). \end{aligned} \tag{A.4}$$

Appendix B. Thermoelastic damping

Solving equation (2) and substituting into equation (3), one finds that

$$\Delta W \approx \frac{\pi \omega_{\mathrm{m}} \alpha^2 E^2 d^5 T_{\mathrm{bath}}}{1080 \kappa_{\mathrm{th}} (1-\sigma)^2} \int \mathrm{d}x\, \mathrm{d}y\, (\nabla^2 \zeta)^2. \tag{B.1}$$

Let us now compare this quantity with the total strain energy U_{mech} given in equation (A.1). For simplicity, here we specialize to the case where the disc has a uniform thickness d, such that

$$U_{\mathrm{mech}} = \frac{E d^3}{24(1-\sigma^2)} \int \mathrm{d}x\, \mathrm{d}y\, \left[(\nabla^2 \zeta)^2 + 2(1-\sigma)\left((\zeta_{xy})^2 - \zeta_{xx}\zeta_{yy}\right)\right]. \tag{B.2}$$

Note that ΔW and U_{mech} have similar forms, as both involve an integral over the membrane area of the quantity $(\nabla^2 \zeta)^2$. The strain energy contains a second term, however, whose relative importance we characterize now. The second term can in fact be re-written as a line integral around the circumference of the membrane,

$$\int \mathrm{d}x\, \mathrm{d}y\, (\zeta_{xy})^2 - \zeta_{xx}\zeta_{yy} = \oint \mathrm{d}x\, \zeta_{xy}\zeta_x - \oint \mathrm{d}y\, \zeta_{yy}\zeta_x. \tag{B.3}$$

This boundary integral vanishes identically for certain types of shapes or boundary conditions, such as a clamped membrane. For our free disc, this boundary term does not identically vanish, but numerically we can confirm that the boundary contribution is small relative to the total strain energy. To a good approximation then we can write $U_{\mathrm{mech}} \approx \frac{Ed^3}{24(1-\sigma^2)} \int \mathrm{d}x\, \mathrm{d}y\, (\nabla^2 \zeta)^2$. This leads to the expression for the thermoelastically limited Q–frequency product given in the main text,

$$Q_{\mathrm{m,th}} f_{\mathrm{m}} = \frac{45 \kappa_{\mathrm{th}}}{\pi E d^2 T_{\mathrm{bath}} \alpha^2} \frac{1-\sigma}{1+\sigma} \left(1 + \frac{U_{\mathrm{opt}}}{U_{\mathrm{mech}}}\right). \tag{B.4}$$

Appendix C. Modification of opto-mechanical coupling strengths

Our theory of optical trapping of membranes predicts dramatic corrections to the simple model of opto-mechanical interactions given by equation (6), when the optical restoring forces (either static or dynamic) become large compared to the natural ridigity of the membrane. In this scenario of strong optical forces, the mechanical mode shape and thus the opto-mechanical coupling strength g become functions of intensity as well, with g generally decreasing with larger intensity. The origin of this effect is intuitively seen by considering a membrane that interacts with a Gaussian cavity mode whose beam waist w is smaller than the membrane radius a. Then, if the optical restoring forces are large compared to the membrane stiffness, the optical beam in fact resembles a new boundary condition that 'pins' the region $r \lesssim w$ of the membrane into place. This reduces the overlap between the mechanical displacement field and the optical beam, and thus g.

This effect is illustrated in figure C.1 for a free SiN membrane of thickness $d = 30\,\mathrm{nm}$ and $a = 25\,\mu\mathrm{m}$, interacting with a beam of waist $w = 15\,\mu\mathrm{m}$. In this calculation the membrane is statically trapped, although a similar effect would occur for sufficiently large dynamical backaction forces as well. In figure C.1(a), we calculate the opto-mechanical coupling strength g (to another cavity mode that has the same beam waist but exhibits an intensity gradient at the

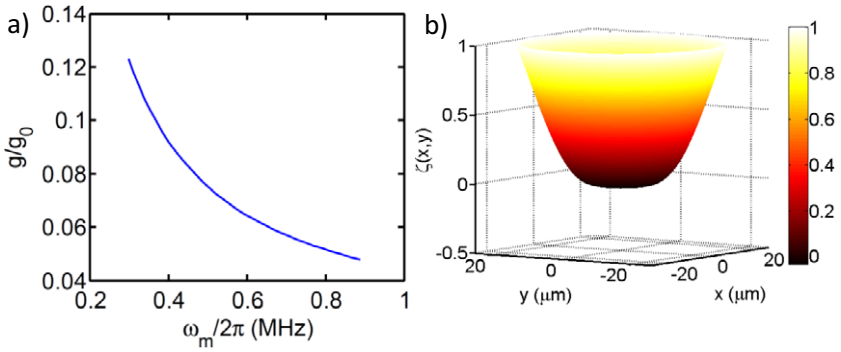

Figure C.1. Effect of large intensity on opto-mechanical coupling strength. (a) Opto-mechanical coupling strength g of a trapped free disc as a function of CM frequency. The coupling strength is normalized by the value corresponding to rigid (pure CM) motion g_0. A decrease in g for increasing frequency is caused by the non-uniform optical force pinning the center of the disc in place. The dimensions for this simulation are $d = 30\,\text{nm}$, $a = 25\,\mu\text{m}$ and $w = 15\,\mu\text{m}$. (b) Displacement field $\zeta(x, y)$ (in arbitrary units) for a free disc of the same dimensions, for a trap frequency of $\omega_\text{m}/2\pi = 300\,\text{kHz}$. The displacement field clearly illustrates the pinning effect created by the optical forces.

membrane position) as a function of the CM frequency, which is varied through the intensity of the trapping beam. The value of g is calculated using the expression [4]

$$g \propto z_\text{zp} \int \text{d}x\,\text{d}y\,\text{e}^{-2(x^2+y^2)/w^2}\zeta(x, y)/\max|\zeta|. \tag{C.1}$$

In figure C.1(a), we have normalized the obtained value of g with the value g_0 if the motion were purely CM, where the displacement field ζ is constant. At larger frequencies, g dramatically decreases, reflecting the 'pinning' effect that the optical force has on the center of the membrane. This is also directly seen in figure C.1(b), where we plot the displacement field $\zeta(x, y)$ for a CM frequency $\omega_\text{m}/2\pi = 300\,\text{kHz}$.

Appendix D. Quantum opto-mechanics with a tethered membrane

In this section, we show that the membrane trapped inside a Fabry–Perot cavity analyzed in section 2 can be cooled to the ground state starting from room temperature under realistic conditions.

To recall, the apodized membrane with radius $r = 9\,\mu\text{m}$ is positioned inside a cavity with nominal beam waist $w_0 \approx 15\,\mu\text{m}$, and we assume that the CM motion is trapped with a frequency of $\omega_\text{m}/(2\pi) = 0.5\,\text{MHz}$ (see table D.1 for a summary of parameters). The corresponding peak circulating intensity of the trapping field is $I_\text{max} \approx 0.04\,\text{W}\,\mu\text{m}^{-2}$. Such a configuration yields a scattering-limited cavity finesse of $\mathcal{F}_\text{mem} \sim 3 \times 10^5$. For our following analysis, we take a more conservative value of $\mathcal{F} = 10^5$ for the overall cavity finesse (e.g. the finesse is limited by the cavity mirror transmission). The corresponding cavity linewidth $\kappa/(2\pi) = 75\,\text{kHz}$ is much smaller than ω_m, ensuring that the 'sideband-resolved regime' is reached and efficient optical cooling can take place [27].

Table D.1. Example cooling parameters for optically trapped membrane.

Cavity length	Beam waist	Opto-mech. coupling strength $g/2\pi$	Cavity finesse F	Total cavity decay $\kappa/2\pi$, membrane contribution $\kappa_{\rm mem}/2\pi$
1.99 cm	15 μm	40 Hz	10^5	75 and 25 kHz
Mech. frequency $\omega_{\rm m}/2\pi$	Intra-cavity intensities: trapping, cooling beams	Background gas pressure	Final phonon number $\langle n_f \rangle$	Final temperature $T_{\rm f}$
0.5 MHz	4×10^{10} and 2×10^6 W m^{-2}	$\sim 10^{-10}$ torr	2.5×10^{-3}	4 μK

The membrane is trapped at an anti-node of the 'primary' mode used for trapping; however, as in [17, 18], a secondary optical cavity mode with a maximum intensity gradient at the membrane position can be used to facilitate linear opto-mechanical coupling and cooling. The theory of cooling in this configuration has been thoroughly analyzed in previous work [17, 18, 34], and the results are briefly summarized here. We assume that the circulating intensity in the secondary mode is a small fraction $\xi \ll 1$ compared to that in the primary mode, so that the trapping (cooling) effect of the secondary (primary) mode is negligible (we take $\xi = 5 \times 10^{-5}$ for our analysis). The optical cooling rate effected by the second mode is obtained from equation (9), with a calculated opto-mechanical coupling strength of $g/(2\pi) = 40$ Hz for our particular geometry. We choose a detuning of $\delta \approx -\omega_{\rm m}$ for our secondary or cooling beam, which maximizes the cooling efficiency in the sideband-resolved regime.

Using these parameters, we find that optical cooling can yield a steady-state phonon occupation number and temperature of $\langle n_f \rangle = 2.5 \times 10^{-3}$ and $T_{\rm f} = 4\,\mu$K, respectively, starting from room temperature. Thus, the ground state of the CM motion can be prepared with extremely high fidelity. So far in our analysis, we have assumed that re-heating of the CM motion occurs due to thermoelastic processes and photon recoil. However, it is known that damping and re-thermalization due to collisions with background gas molecules can be a major decoherence effect for levitated systems [17, 18]. In the low-pressure regime, where gas molecules independently collide with the membrane, the energy damping rate for our system can be derived using the techniques of [35] and is given by $\gamma_{\rm g} = 96 P_{\rm g}/(\pi \bar{v} \rho d_0)$, where $P_{\rm g}$ is the gas pressure, $\bar{v}$ is the mean molecular speed, ρ is the mass density of the membrane and d_0 is its maximum thickness. For our system, the effect of the background gas is negligible compared to other heating sources at pressure levels of $P_{\rm g} \sim 10^{-10}$ torr.

References

[1] Cleland A 2009 Optomechanics: photons refrigerating phonons *Nature Phys.* **5** 458–60
[2] Teufel J D, Donner T, Li D, Harlow J W, Allman M S, Cicak K, Sirois A J, Whittaker J D, Lehnert K W and Simmonds R W 2011 Sideband cooling of micromechanical motion to the quantum ground state *Nature* **475** 359–63
[3] Chan J, Alegre T P M, Safavi-Naeini A H, Hill J T, Krause A, Groblacher S, Aspelmeyer M and Painter O 2011 Laser cooling of a nanomechanical oscillator into its quantum ground state *Nature* **478** 89–92
[4] Wilson D J, Regal C A, Papp S B and Kimble H J 2009 Cavity optomechanics with stoichiometric SiN films *Phys. Rev. Lett.* **103** 207204

[5] Marshall W, Simon C, Penrose R and Bouwmeester D 2003 Towards quantum superpositions of a mirror *Phys. Rev. Lett.* **91** 130401
[6] Genes C, Mari A, Tombesi P and Vitali D 2008 Robust entanglement of a micromechanical resonator with output optical fields *Phys. Rev.* A **78** 032316
[7] Chang D E, Safavi-Naeini A H, Hafezi M and Painter O 2011 Slowing and stopping light using an optomechanical crystal array *New J. Phys.* **13** 023003
[8] Geraci A A, Papp S B and Kitching J 2010 Short-range force detection using optically cooled levitated microspheres *Phys. Rev. Lett.* **105** 101101
[9] Li T, Kheifets S, Medellin D and Raizen M G 2010 Measurement of the instantaneous velocity of a Brownian particle *Science* **328** 1673–5
[10] Verbridge S S, Parpia J M, Reichenbach R B, Bellan L M and Craighead H G 2006 High quality factor resonance at room temperature with nanostrings under high tensile stress *J. Appl. Phys.* **99** 124304
[11] Lee J E-Y and Seshia A A 2009 5.4 MHz single-crystal silicon wine glass mode disk resonator with quality factor of 2 million *Sensors Actuators* A **156** 28–35
[12] Lifshitz R and Roukes M L 2000 Thermoelastic damping in micro- and nanomechanical systems *Phys. Rev.* B **61** 5600–9
[13] Pohl R O, Liu X and Thompson E 2002 Low-temperature thermal conductivity and acoustic attenuation in amorphous solids *Rev. Mod. Phys.* **74** 991–1013
[14] Ashkin A 2007 *Optical Trapping and Manipulation of Neutral Particles Using Lasers: A Reprint Volume with Commentaries* (Singapore: World Scientific)
[15] Ashkin A and Dziedzic J M 1976 Optical levitation in high vacuum *Appl. Phys. Lett.* **28** 333–5
[16] Libbrecht K G and Black E D 2004 Toward quantum-limited position measurements using optically levitated microspheres *Phys. Lett.* A **321** 99–102
[17] Chang D E, Regal C A, Papp S B, Wilson D J, Ye J, Painter O, Kimble H J and Zoller P 2010 Cavity opto-mechanics using an optically levitated nanosphere *Proc. Natl Acad. Sci. USA* **107** 1005–10
[18] Romero-Isart O, Juan M L, Quidant M L and Cirac J I 2010 Toward quantum superposition of living organisms *New J. Phys.* **12** 033015
[19] Sankey J C, Yang C, Zwickl B M, Jayich A M and Harris J G E 2010 Strong and tunable nonlinear optomechanical coupling in a low-loss system *Nature Phys.* **6** 707–12
[20] Landau L D and Lifshitz E M 1986 *Theory of Elasticity* 3rd edn (Boston, MA: Butterworth-Heinemann)
[21] Penn S D, Ageev A, Busby D, Harry G M, Gretarsson A M, Numata K and Willems P 2006 Frequency and surface dependence of the mechanical loss in fused silica *Phys. Lett.* A **352** 3–6
[22] Fox A G and Li T 1968 Computation of optical resonator modes by the method of resonance excitation *IEEE J. Quantum Electron.* **4** 460–5
[23] Li Yu, Huang M, Chen M, Chen W, Huang W and Zhu Z 1998 Quasi-discrete Hankel transform *Opt. Lett.* **23** 409–11
[24] Born M, Wolf E and Bhatia A B 2000 *Principles of Optics: Electromagnetic Theory of Propagation, Interference and Diffraction of Light* (Cambridge: Cambridge University Press)
[25] Braginsky V B and Vyatchanin S P 2002 Low quantum noise tranquilizer for Fabry–Perot interferometer *Phys. Lett.* A **293** 228–34
[26] Corbitt T, Chen Y, Innerhofer E, Müller-Ebhardt H, Ottaway D, Rehbein H, Sigg D, Whitcomb S, Wipf C and Mavalvala N 2007 An all-optical trap for a gram-scale mirror *Phys. Rev. Lett.* **98** 150802
[27] Marquardt F, Chen J P, Clerk A A and Girvin S M 2007 Quantum theory of cavity-assisted sideband cooling of mechanical motion *Phys. Rev. Lett.* **99** 093902
[28] Jayich A M, Sankey J C, Zwickl B M, Yang C, Thompson J D, Girvin S M, Clerk A A, Marquardt F and Harris J G E 2008 Dispersive optomechanics: a membrane inside a cavity *New J. Phys.* **10** 095008
[29] Nunnenkamp A, Børkje K, Harris J G E and Girvin S M 2010 Cooling and squeezing via quadratic optomechanical coupling *Phys. Rev.* A **82** 021806
[30] Singh S, Phelps G A, Goldbaum D S, Wright E M and Meystre P 2010 All-optical optomechanics: an optical spring mirror *Phys. Rev. Lett.* **105** 213602

[31] Meystre P, Wright E M, McCullen J D and Vignes E 1985 Theory of radiation-pressure-driven interferometers *J. Opt. Soc. Am.* B **2** 1830–40
[32] Boyd R W 1992 *Nonlinear Optics* (New York: Academic)
[33] Rosenberg J, Lin Q and Painter O 2009 Static and dynamic wavelength routing via the gradient optical force *Nature Photonics* **3** 478–83
[34] Pender G A T, Barker P F, Marquardt F and Monteiro T S 2011 Optomechanical cooling of levitated spheres with doubly-resonant fields, arXiv:1107.0686
[35] Hutcherson S and Ye W 2004 On the squeeze-film damping of micro-resonators in the free-molecule regime *J. Micromech. Microeng.* **14** 1726–33